ACS OMEGA

http://pubs.acs.org/journal/acsodf

Article

Effect of Pressure on Burning and Soot Characteristics of RP-3 Kerosene Droplets under Sub-Atmospheric Pressure

Jie Huang, Yong He, Hongtao Zhang, Yan Dai, and Zhihua Wang*

Cite This: *ACS Omega* 2023, 8, 14053−14065

Read Online

ACCESS | Metrics & More | Article Recommendations

ABSTRACT: The burning and soot characteristics of RP-3 kerosene droplets under sub-atmospheric pressure were experimentally investigated in a pressure chamber. The droplet size during combustion was continuously recorded using a high-speed camera, and the burning rate based on the d^2− law was determined. The flame temperature was calculated from ICCD camera spectral data using two-color pyrometry, and the carbon soot volume fraction was measured by the calibrated laser-induced incandescence (LII) technique. Soot particles were also sampled using a thermophoretic deposition probe and characterized using a transmission electron microscope (TEM) for particle size and morphology. The results showed that the droplet burning rate increased monotonically with increasing pressure under sub-atmospheric pressure, and the flame temperature slightly decreased with increasing pressure. Sub-atmospheric pressure environment significantly inhibits the formation of soot particle clusters during the ignition of droplets. The average soot volume fraction in the flame increases approximately with increasing pressure at 0.2−1.0 bar with a power of 2.044 ± 0.066. As the pressure decreases from 1.0 to 0.2 bar, the average soot volume fraction decreases significantly from 11.801 to 0.437 ppm. This is mainly due to the fact that the sub-atmospheric environment not only inhibits the collision growth of soot particles but also promotes the oxidation process of soot particles. The collected soot particles reveal a significant reduction in particle size under sub-atmospheric pressure with average primary soot particles of 48.23, 40.06, 27.096, and 18.718 nm at 1.0, 0.6, 0.4, and 0.3 bar pressures, respectively. The change in the number density of carbon soot particles is not significant, which reveals that the change in the diameter of soot particles under sub-atmospheric pressure plays a key role in the change in the volume fraction of soot.

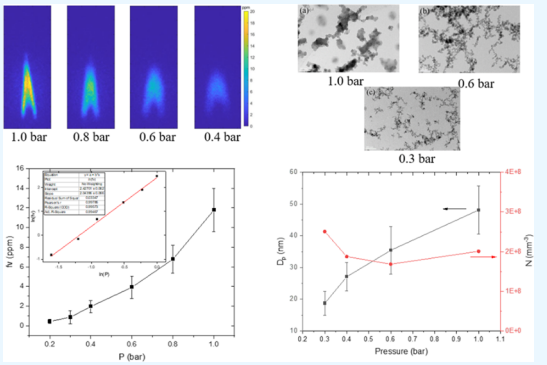

1. INTRODUCTION

Ramjet is a new advanced aerospace science and technology for high-speed flight. With the development of the technology, higher demands are focused on the ability of ramjet engines to operate at high altitudes, high speed, and wide range. At high altitudes, due to thin air, ramjet engines ingest low mass airflow rates at reduced pressure values in the combustion chamber.[1] When the inlet pressure of the combustion chamber is reduced to less than one atmosphere, the stability and efficiency of combustion will deteriorate.[2] However, most of the current studies on the evaporation and combustion characteristics of liquid fuel under elevated temperature are conducted at elevated pressure[3−6] or atmospheric pressure[7−9] environments. Investigating the combustion of liquid fuel under sub-atmospheric pressure is essential to improve the working stability of ramjet at high altitudes. Previous research work[10,11] has revealed the evaporation rate, ignition time, OH distribution, and micro-explosion characteristics at sub-atmospheric pressure, revealing that the effect of sub-atmospheric pressure environment on droplet combustion behavior is significant.

Soot, as a product of incomplete combustion, is widely present in the combustion process of various hydrocarbon fuels. Soot could cause a decrease in the operating efficiency of combustion equipment, fine particles causing pollution and other hazards,[12,13] and also has a direct impact on the radiation characteristics of the flame and the evaporation characteristics[14] of a droplet. Abdul Rasid and Zhang[15] examined the effect of soot pollution on the combustion characteristics and liquid-phase visualization of a single diesel droplet. They found that soot contamination reduced the combustion rate of pure diesel droplets by 17%. And the higher the degree of soot contamination on the droplet surface, the greater the destructive behavior on surface deformation and flame formation, implying that soot concentration has a non-

Received: February 1, 2023
Accepted: March 28, 2023
Published: April 6, 2023

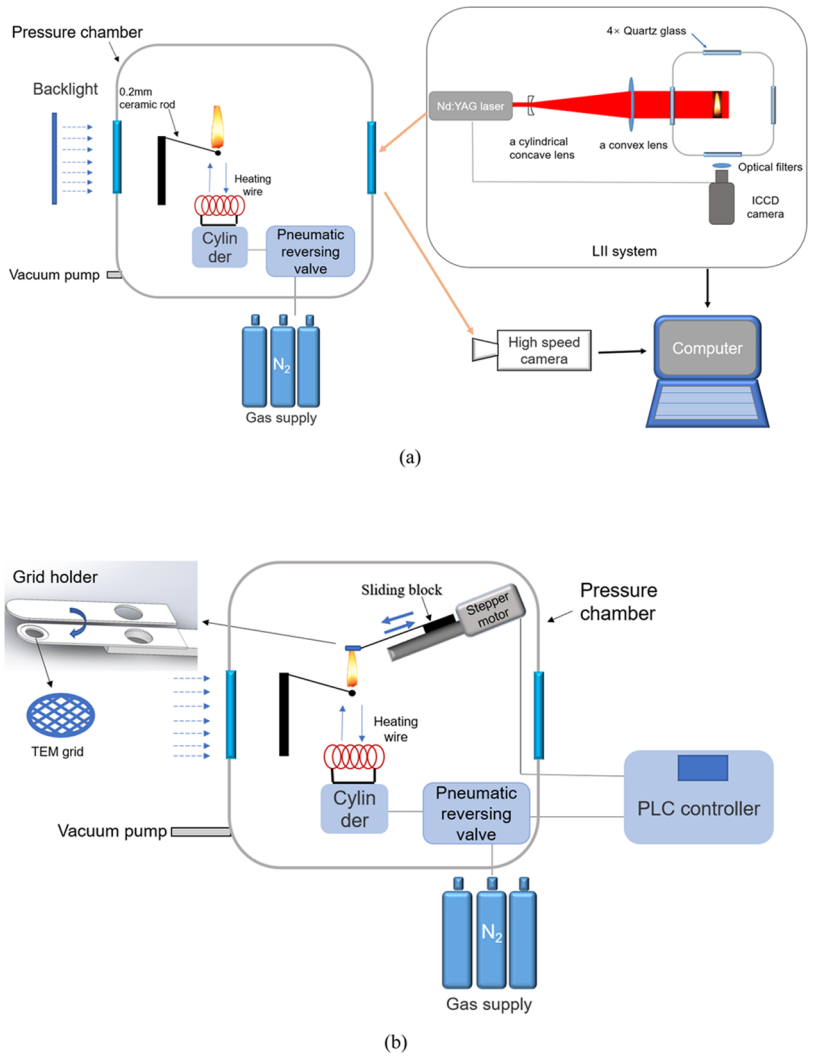

Figure 1. Schematic of experimental setup: (a) single-droplet combustion apparatus; and (b) soot sampling technique.

negligible effect on the droplet characteristics in spray combustion.

However, due to the short duration of droplet combustion (1−2 s), studies on the characteristics of soot generation from droplet combustion have been mostly limited to qualitative studies. Jackson et al.[16] observed the formation of soot shells and found that the vaporization rate of monochlorinated alkane droplets was slower, which resulted in their soot shells being closer to the droplet surface than those of *n*-heptane. Zhu et al.[17,18] investigated the effect of *n*-butanol addition to diesel/biodiesel blends and oxygenates addition to diesel on soot generation from single-droplet combustion. They determined the intensity of soot expressed by the KL factor by analyzing the optical spectrum of CCD camera images using two-color thermometry. Other researchers[4,5,9,19,20] have also studied the characteristics exhibited by droplets in combustion, but the optical diagnostic capabilities in these studies were limited to blackbody radiation by soot. It is worth noting that the spontaneous radiation signal is accumulated from different radii of the droplet flame, and the morphological changes of the flame (which are common in droplet combustion) can very easily interfere with the signal. Although it is theoretically possible to calculate the signal on the central cross section of flame by the Abel transform of Dasch et al.,[21] however, the transient, unstable, and deviating from axisymmetric characteristics of the droplet flame increase the error of the calculation significantly. No similar applications have been reported so far. Planar laser-induced incandescence (PLII) has been widely used for the quantitative measurement of soot volume concentration.[22−24] PLII uses a high-energy laser to heat soot particles to 4000 K and then emits near-blackbody radiation. The magnitude of the incandescent signal is proportional to the soot concentration, combined with the laser extinction method grams to quantitatively obtain the concentration of soot on the laser cross section.[24] After laser extinction method calibration, the soot concentration on the laser cross section can be obtained quantitatively. Compared to other means of detection, PLII stands out due to its high dynamic range. The system provides reliable measurements of extremely low and high soot concentrations without any special modifications.[25] This is important in studies examining the effect of pressure on soot due to the very large variation of soot concentration with pressure.[26] However, since radiation becomes the main heat transfer mechanism for soot particles in a sub-atmospheric environment, the temperature decay rate does not provide information on soot particle size.[27] Therefore, PLII has difficulties in measuring the particle size of soot under sub-atmospheric pressure. On the other hand,

https://doi.org/10.1021/acsomega.3c00655
ACS Omega 2023, 8, 14053−14065

the thermophoretic deposition technique and electron microscopy have been widely used to measure the particle size and morphology of soot in laminar diffusion flames,[28,29] turbulent diffusion flames,[30] engines,[31] and droplet flames,[17] which also offer the possibility of measuring the particle size of soot at sub-atmospheric pressure.

Although the fuel is more likely to be burned at variable pressure conditions, most of the current studies on soot generation from fuels are conducted at atmospheric pressure.[23,28] Quantitative measurements of the effect of pressure on the soot concentration from single-droplet combustion have not been reported. A few researchers have investigated the effect of pressure on soot generation from laminar diffusion flames.[25] Joo and Gülder[26] studied soot generation from methane-air laminar diffusion flames at high pressure and found that the maximum soot volume fraction increased from 14 ppm at 10 atm to 180 ppm at 60 atm. Flower and Bowman[32] studied ethylene/air laminar diffusion flames at 1−2.5 bar and observed that maximum and integrated soot volume fractions increased approximately as the pressure raised to a power of 1.7 ± 0.3.

The suspended single-droplet combustion approach with electric heater wires was adopted because of its simplicity and the ease of intervention of measuring instruments. The burning rate, soot volume concentration, soot particle size, and nanostructure of RP-3 droplets in sub-atmospheric pressure are systematically examined.

2. EXPERIMENTAL APPARATUS

A schematic of the experimental apparatus is shown in Figure 1a. A pump is connected to the pressure chamber through a pipe to pump air from the chamber to create a sub-atmospheric pressure environment. The cylinder is controlled by a time delay relay to push the heating wire close to the liquid droplet for ignition. A DC-regulated power supply is used to provide 3.6A DC power to the heater wire to ensure the stability of the wire temperature. A micro-pipette (2.0 μL) is used to generate a droplet and placed on the end of a 0.2 mm diameter zirconia ceramic rod. Compared with commonly used thermocouple[10,33] and SiC ceramic rod[5,9] [5.2 W/(m K)], the zirconia ceramic rod has much lower thermal conductivity [1−2 W/(m K)], which can reduce heat transfer to the droplet. Four optical windows are designed around the pressure chamber walls for light to pass through, allowing for laser diagnosis and optical observation.

Optical measurement methods used here include LII (laser-induced incandescent light) detection, high-speed camera technology, and color digital single lens reflex (DSLR) camera. The LII measurement system includes a Nd:YAG laser (Spectra Physics, Pro-250-10H), a cylindrical concave lens, a convex lens, and an ICCD camera (Princeton Instrument, PI-MAX4). The laser light (1064 nm) output from the Nd:YAG laser with a frequency of 10 Hz was used as the light source for the LII experiment. The laser was formed into a laser sheet by the use of a cylindrical concave lens and a convex lens. The laser sheet passes through the quartz window and across the central axis of the droplet burning flame. The carbon soot particles in the flame were excited to an incandescent state (roughly 4000 K). The intense radiant light emitted was captured by an ICCD camera placed perpendicular to the laser sheet after passing through the quartz window. The ICCD camera was equipped with a bandpass filter (FWHM = 10 nm) with a central wavelength of 430 nm in front of the camera. The gate delay and gate width were set to 130 and 40 ns, respectively. The co-flow burner for LII calibration measurements consists of a central fuel tube of 6 mm diameter and an outer tube of 30 mm diameter. The outer tube was filled with porous ceramic and stainless steel microbeads of 3 mm diameter. The ethylene flow rate was set at 0.28 std L/min, and the airflow rate used to stabilize the diffusion flame was 1.8 std L/min. The burner was placed inside the pressure chamber during calibration to eliminate the influence of the quartz window on the measurement. The average value of soot concentration at different heights of the ethylene flame was measured by the extinction method, and when combined with the LII signal, the ratio of the soot volume concentration to the LII signal value can be obtained.

Soot flame temperature was measured by the two-color pyrometry. In order to acquire the signal of droplet transient flame spontaneous emission at dual wavelengths simultaneously, a spectroscope (VZ-image doubler, LAVISION) was mounted in front of the ICCD camera. At the same time, two central wavelengths of 532 and 647 nm filters (FWHM = 1 nm) were added to the lens. The exposure time of the camera was set to 500 μs. For calibration of two-color temperature measurement system parameters by S-type thermocouples, it was placed in a high-temperature environment. To avoid the influence of the quartz window of the pressure chamber on the temperature measurement system, the thermocouple for calibration was placed in the chamber near the droplet flame.

A black and white high-speed camera (IDT Y4-S1) was used at a frame rate of 3000 Hz to capture the carbon smoke shape and the rapid change in droplet diameter during evaporation and micro-explosion. The exposure time was set to 20 μs. The lens used was Sigma 200 mm Macro Lens. A DSLR camera (Canon 77D) was used to capture the color and shape of the flames at 50 Hz. A Matlab code was used to evaluate the droplet projection area $S_p(t)$ in the shooting direction at each moment, so as to obtain the droplet diameter results calculated by $D(t) = \sqrt{4S_p(t)/\pi}$. Chinese RP-3 kerosene was chosen as the fuel for the experiment. It typically consists of 52.2% of alkanes, 39.9% of naphthenes, and 7.9% of aromatic hydrocarbons, by mass,[10] and the fractions with more than 2% content measured by chromatography-mass spectrometry can be referred to our previous study.[11]

Soot was sampled using the thermophoretic deposition technique.[17,28,34] The thermophoretic sampling equipment and combustion system are shown in Figure 1b. It consists of a sampling module, motor drive module, and control module. To ensure a good sealing of the pressure chamber, the motor drive module and the sampling module are placed inside the pressure chamber. They are connected to the control module outside the chamber via a wire connection at the bottom of the pressure chamber. The sampling module is made of two 0.25 mm thick stainless steel plates to reduce the disturbance of flame during the sampling process,[35] which is more critical for the small scale generated by droplet combustion. One of the pieces has a 3.1 mm diameter and 0.05 mm deep groove for placing the TEM grid (a C/Cu TEM grid with 200 mesh, 3 mm in diameter), and a sampling hole of 2 mm diameter is drilled on another piece to collect the soot particles in the TEM grid due to thermal diffusion phenomenon. The motor drive module is composed of a stepper motor and a slider, which can quickly transport the sampling module in a straight line into the droplet flame and leave after 0.05 s. Due to the

https://doi.org/10.1021/acsomega.3c00655
ACS Omega 2023, 8, 14053−14065

short droplet burning duration of 1−2 s, time synchronization between the ignition system and the sampling system is necessary. A PLC controller (DKC-Y240) is used to simultaneously control stepper motors and output 24 V DC signals. The 24 V DC signal is converted to 220 V AC through an intermediate relay to control the ignition process of the cylinder drive. During the experiment, the sampling system starts to operate after the ignition wire is withdrawn for 0.2 s. The soot morphological features were examined using a FEI Tecnai G2 F20 transmission electron microscopy (TEM) with the accelerating voltage of 200 kV to obtain TEM images, which were analyzed using the Image-Pro Plus software.

3. RESULTS AND DISCUSSION

3.1. Burning Rate and Soot Flame Temperature. The temporal changes in the square of the normalized droplet diameter of RP-3 under 0.2−1.0 bar as well as calculated burning rates are shown in Figure 2. It is obvious from Figure 2a that, except for the 0.2 bar pressure, the droplet diameters at the rest of the pressure are entering a smooth evaporation period after the initial heating and fluctuation evaporation period. Overall, the RP-3 droplet size at 0.4−1.0 bar pressure basically varies linearly with time, indicating that droplet combustion conforms to the d^2−law. There were significant fluctuations in droplet size after the initial heating period, and both the magnitude and frequency of the fluctuations increased significantly with decreasing pressure. This is due to the fact that the boiling points of low boiling components such as hexane,2,5-dimethyl-(382.1 ± 0.9 K), cyclohexane,1,3-dimethyl-,cis-(393 ± 1 K), and heptane,3-methyl-(392 ± 1 K) within RP-3 are much lower than the boiling points of high boiling components such as nonadecane (602.9 K), pentadecane (540 ± 20 K), and tetradecane (523 ± 10 K).[11] In a high-temperature environment, the lower boiling components evaporate preferentially. The concentration of high boiling components on the surface increases, creating a localized superheated environment inside the droplet that causes bubbles to nucleate, grow, merge, and rupture.[36] Sub-

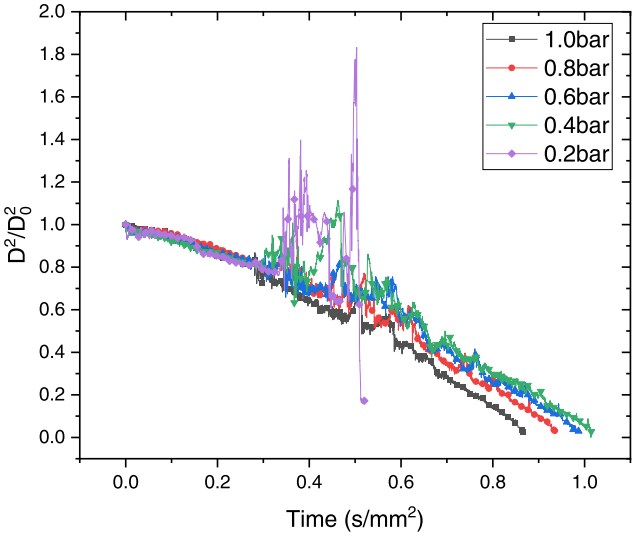

(a)

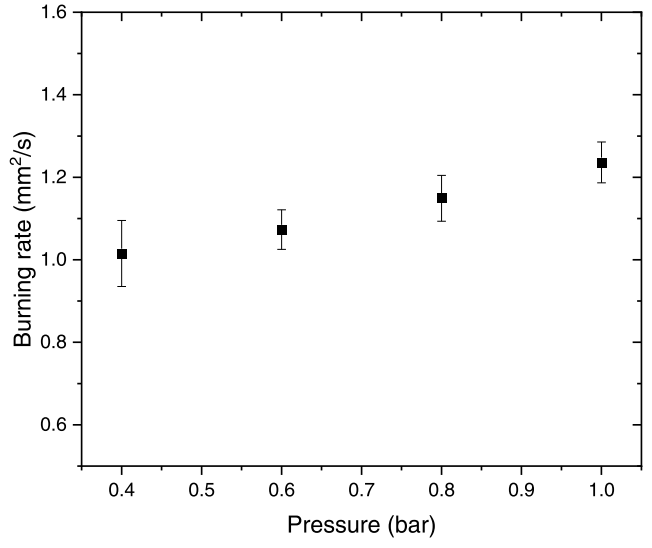

(b)

Figure 2. Experimental results: (a) temporal variation of the normalized D^2 and (b) burning rates.

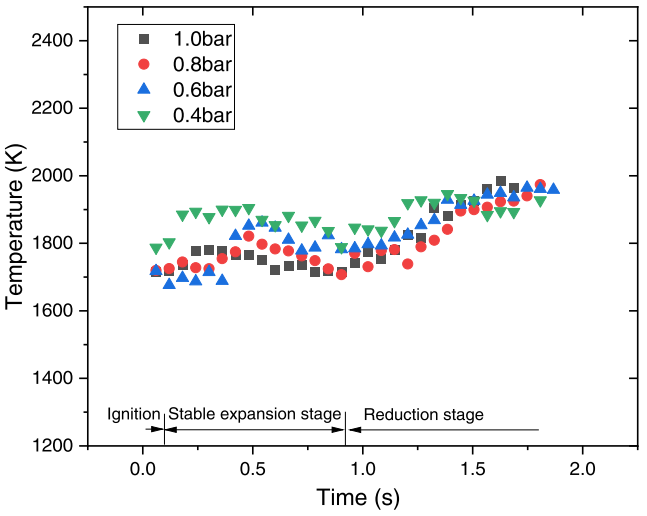

(a)

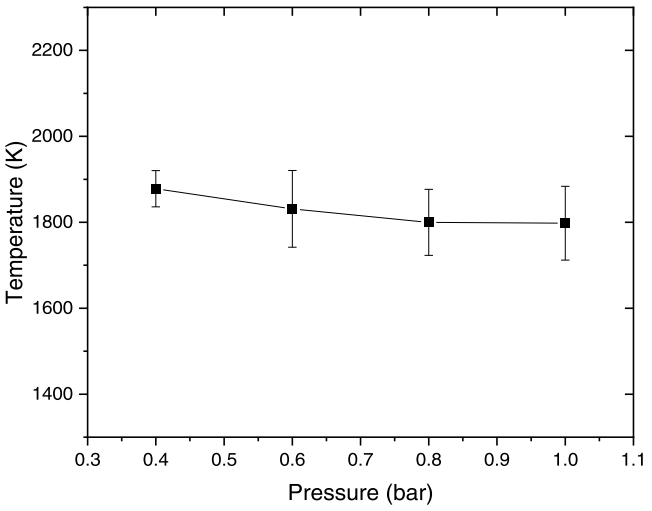

(b)

Figure 3. Experimental results: (a) temporal variation of the soot flame temperature and (b) its time average.

https://doi.org/10.1021/acsomega.3c00655
ACS Omega 2023, 8, 14053−14065

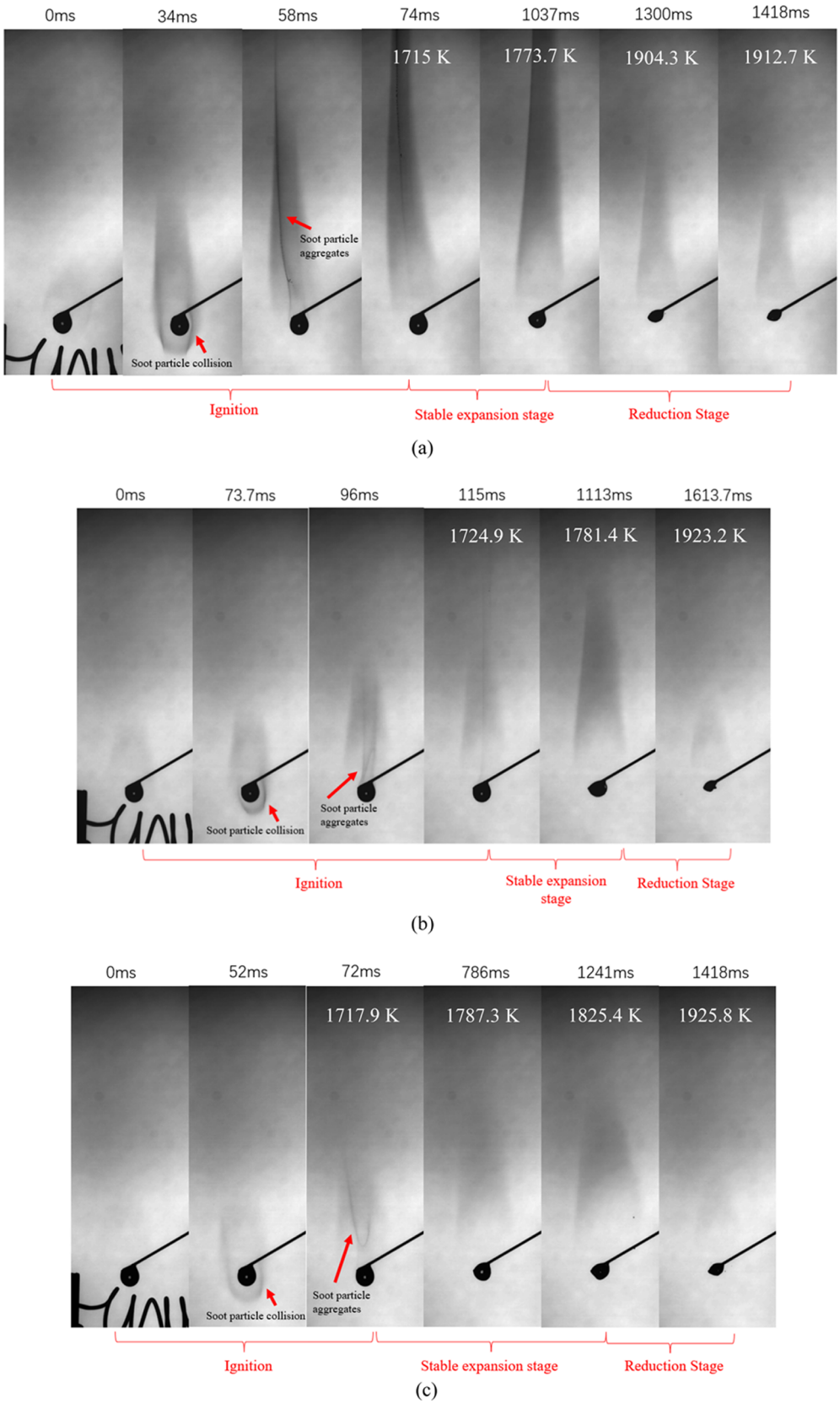

Figure 4. Droplet soot release process captured by a high-speed camera under (a) 1.0 bar; (b) 0.8 bar; (c) 0.6 bar.

atmospheric pressure environments significantly increase the bubble growth rate, resulting in more intense diameter changes.[10] The data shown in Figure 2a were linearly fit to obtain the burning rates, and the standard deviation of the repeated measured burning rate is the error, as shown in Figure 2b (each measurement was repeated at least three times). It is obvious that the burning rate decreases gradually with decreasing pressure. The combustion rate decreases from

https://doi.org/10.1021/acsomega.3c00655
ACS Omega 2023, 8, 14053−14065

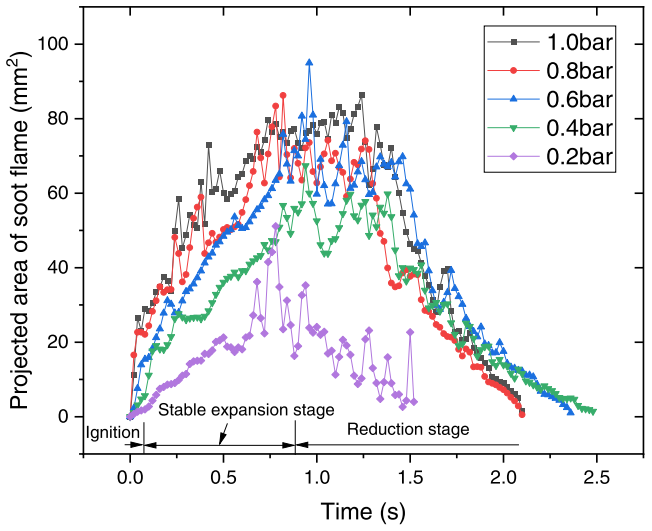

Figure 5. Variation of projected area of soot flame under 0.2−1.0 bar.

1.236 to 1.015 mm^2/s when the ambient pressure decreases from 1.0 to 0.4 bar. The soot flame temperature measured by the two-color method is shown in Figure 3a. As droplet combustion proceeds, especially after entering the flame reduction stage, the soot flame temperature gradually increases, and the pressure change has relatively little effect on the soot flame temperature. This is why the trend of combustion rate with pressure is the same as the trend of evaporation rate found in previous studies.[11] They are both due to the fact that although the boiling point of each component decreases with decreasing pressure thus promoting evaporation, the deterioration of heat transfer due to sub-atmospheric pressure has a greater effect on the combustion/evaporation rate. The temperature of Figure 3b is obtained by averaging the data of Figure 3a with the standard deviation of the error bars. It can be found that the flame temperature increases slightly with decreasing pressure. As the pressure dropped from 1.0 to 0.4 bar, the flame temperature increased from 1798 to 1878 K. A similar phenomenon was found in the study of high-pressure laminar methane-air diffusion flames.[29] In general, the flame temperature of droplets is determined by the oxidant concentration, the burning rate, and the radiant heat loss of the gas and soot in the flame. On the one hand, the low-pressure environment not only reduces the oxygen molecular density but also decreases the burning rate of RP-3 droplets as shown in Figure 2, which will lower the flame temperature. However, on the other hand, because the low-pressure environment significantly reduces the soot intensity, the overall soot radiation loss is reduced, which will increase the flame temperature. In addition, the enhanced OH* chemiluminescence intensity in sub-atmospheric environment found in previous studies[10] also favors the increase of flame temperature. The balance of these opposite effects led to the slight increase in flame temperature with decreasing pressure observed in this experiment.

3.2. Soot Characteristics. *3.2.1. Soot Emission Stage during Droplet Combustion.* The images captured by the high-speed camera are processed with increased contrast to allow for clearer observation of the attenuation of the backlight after it has passed through the soot flame. The processed image

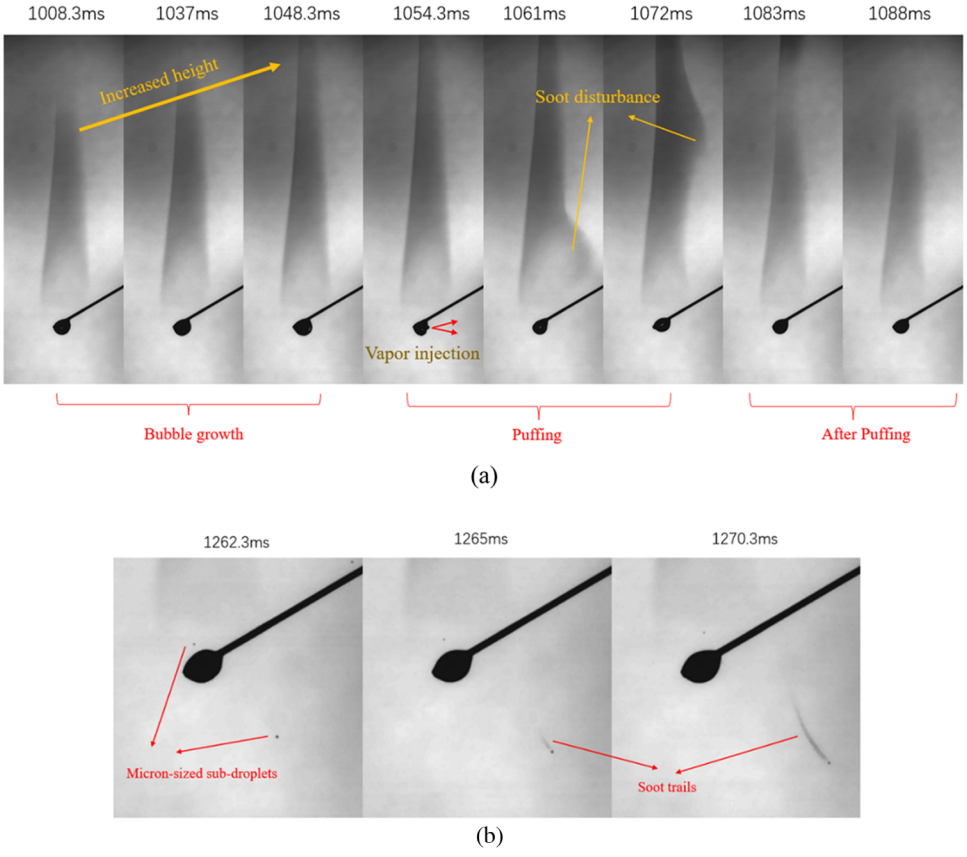

Figure 6. Soot characteristics of (a) puffing and (b) sub-droplets (1.0 bar).

https://doi.org/10.1021/acsomega.3c00655
ACS Omega 2023, 8, 14053−14065

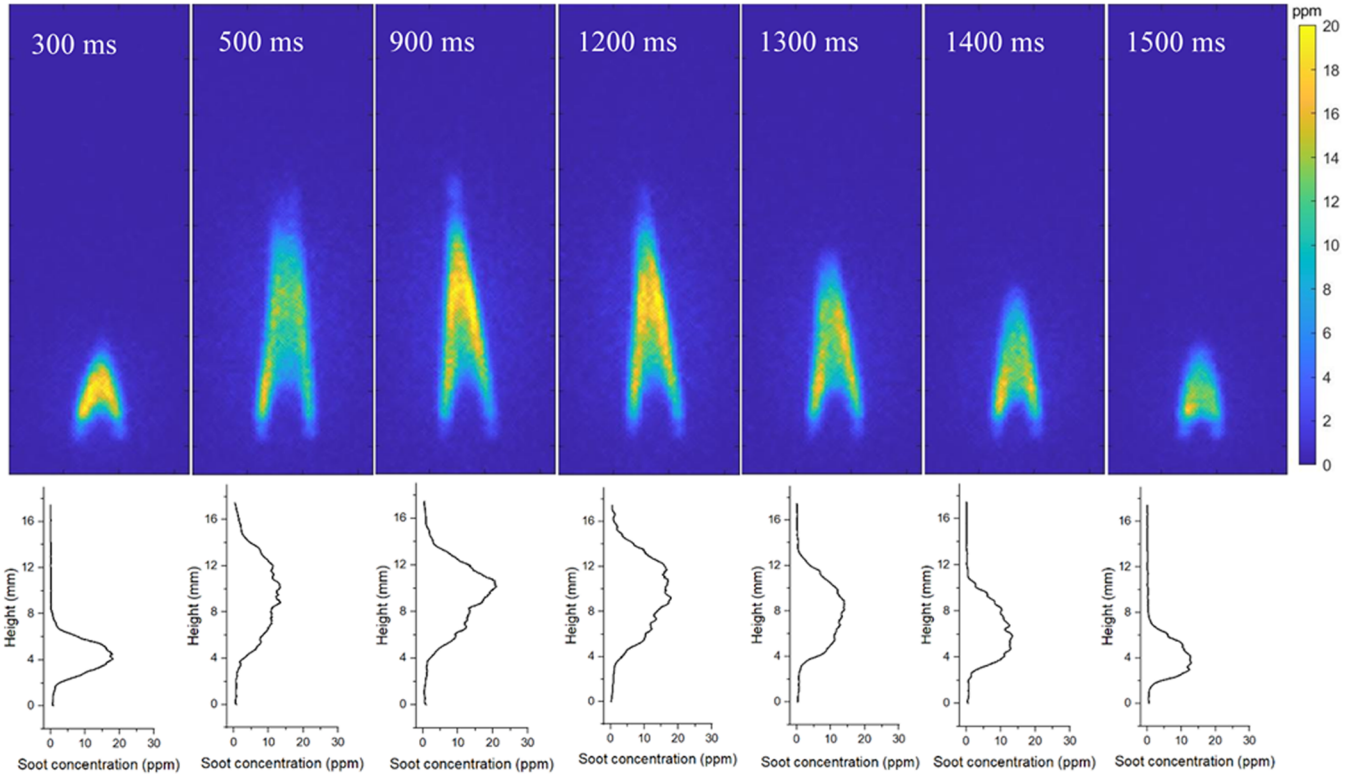

(a)

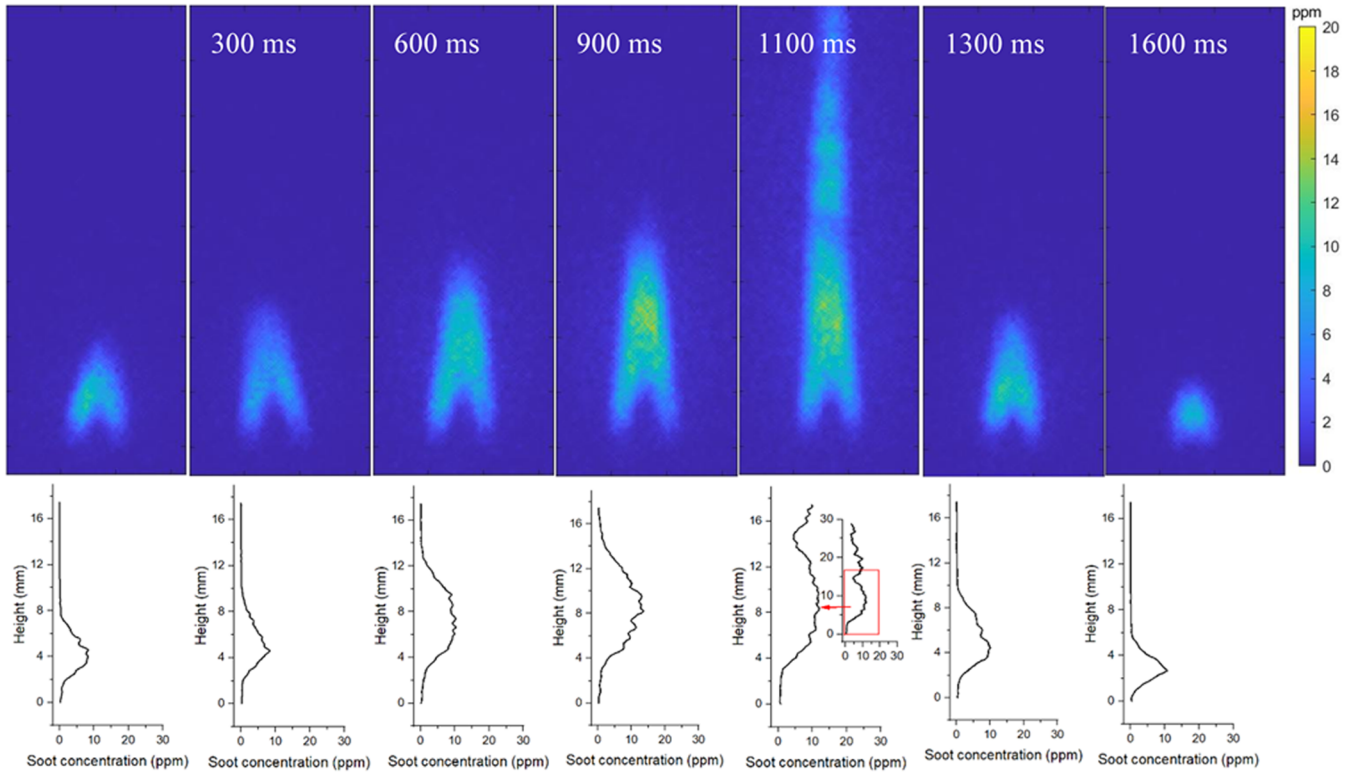

(b)

Figure 7. continued

https://doi.org/10.1021/acsomega.3c00655
ACS Omega 2023, 8, 14053−14065

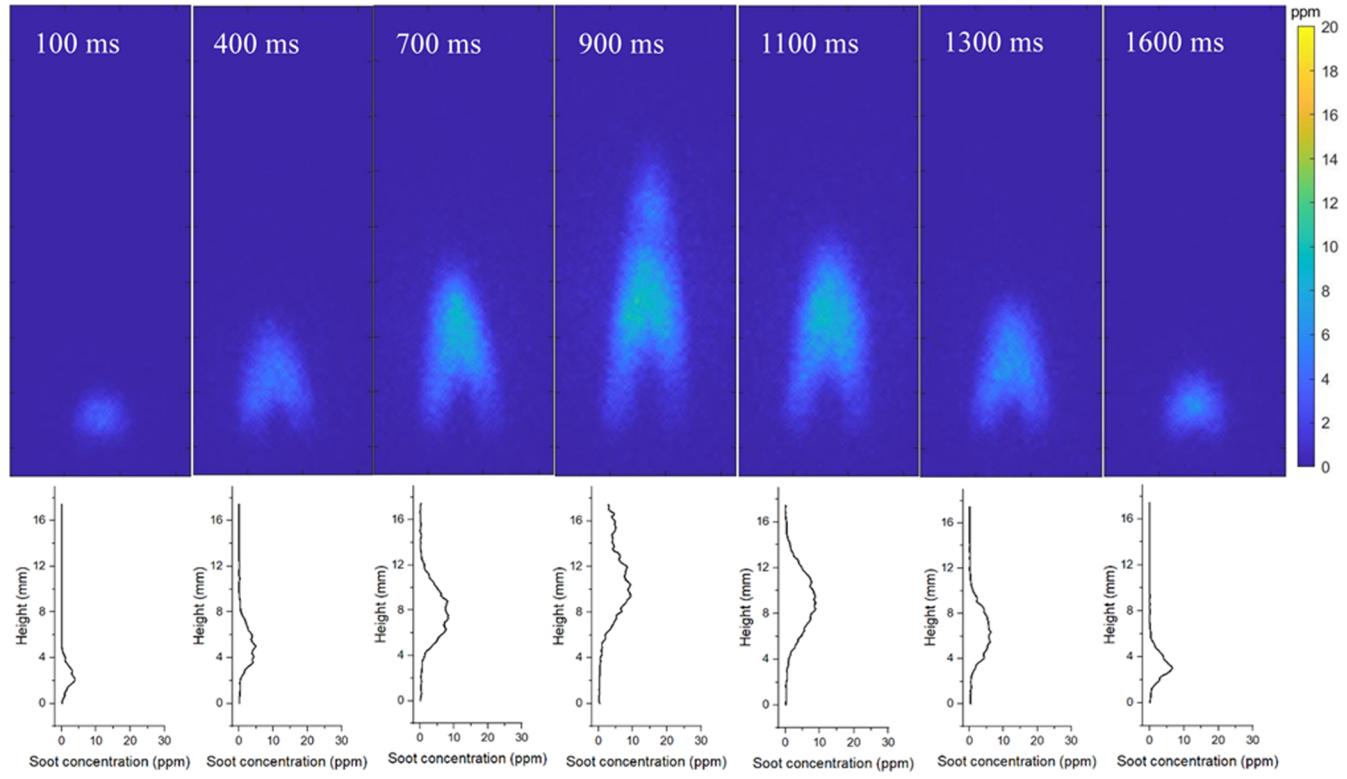

(c)

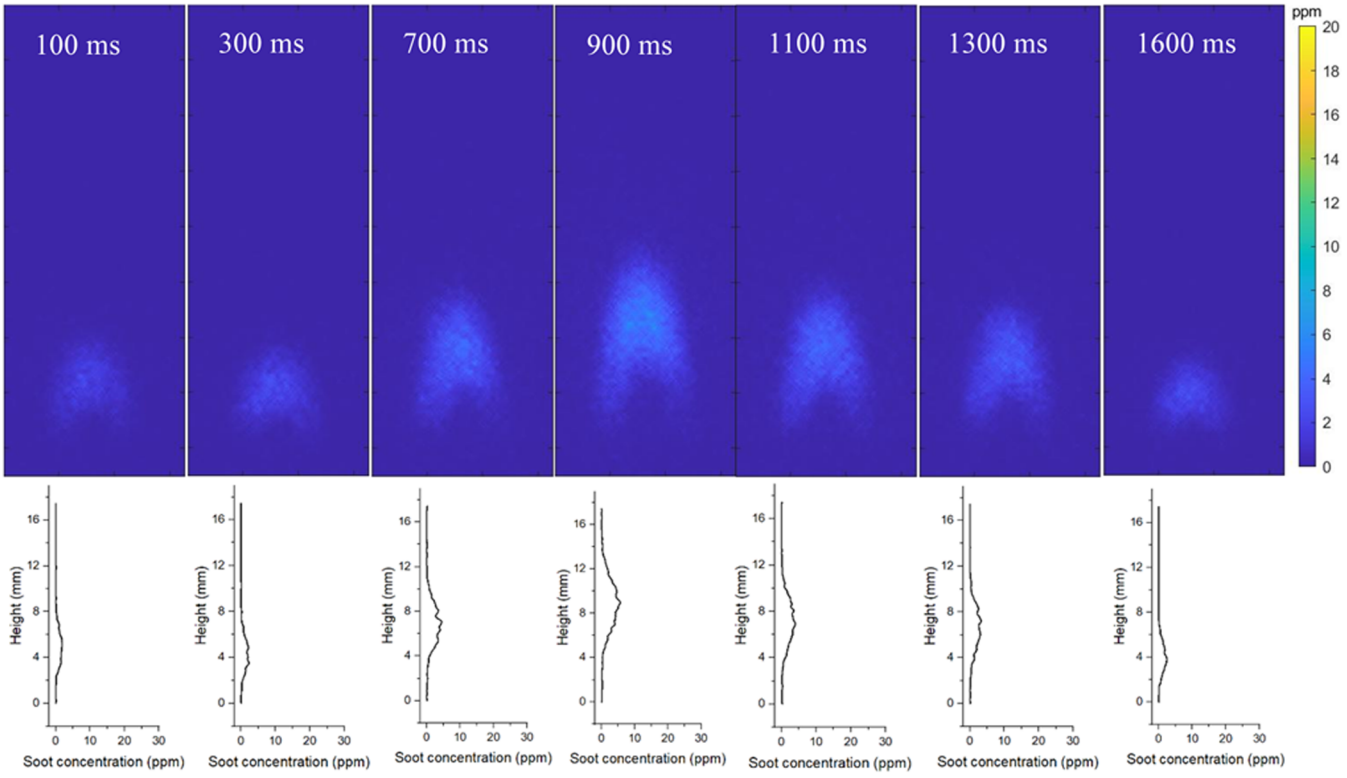

(d)

Figure 7. Soot concentration distribution of the droplet flame at (a) 1.0 bar, (b) 0.8 bar, (c) 0.6 bar, and (d) 0.4 bar.

is shown in Figure 4. The soot flame throughout the droplet combustion can be divided into three stages: (1) ignition, (2) stable expansion, and (3) reduction stage. First of all, it is clear that the ignition process has an impact on the soot emission

https://doi.org/10.1021/acsomega.3c00655
ACS Omega 2023, 8, 14053−14065

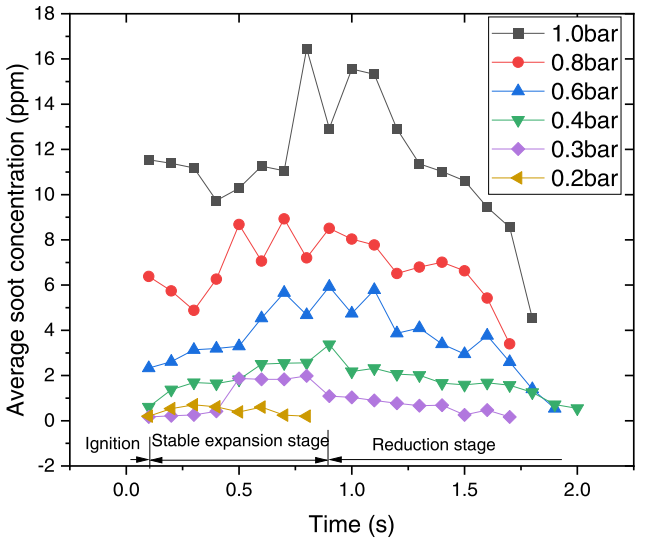

(a)

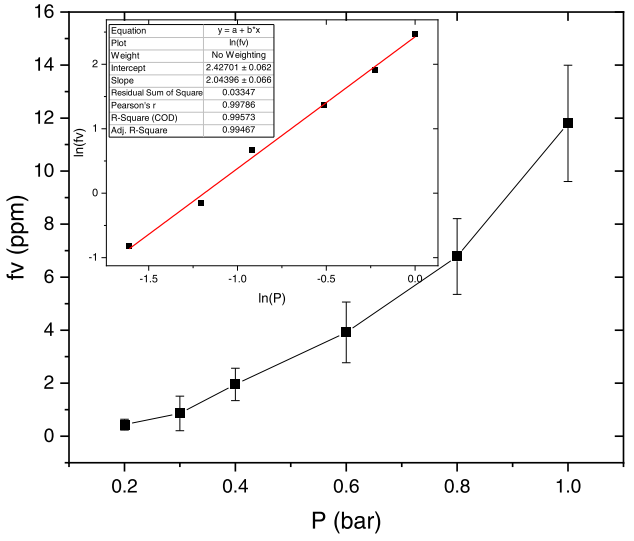

(b)

Figure 8. Experimental results: (a) average soot concentration of the droplet flame and (b) its time average, f_v.

characteristics of the droplets. After the electric wire below the droplet is removed, the flow field around the droplet changes to promote the collision between carbon soot particles and the formation of soot aggregates locally, and the decrease in pressure significantly inhibits the formation of carbon soot aggregates as shown in Figure 4. Then the flame began to continue to expand until 800−1200 ms to reach the maximum flame area. It is clear that the reduced pressure slows down the flame expansion rate and the maximum flame area as shown in Figure 5. This is due to the lower natural convection and lower soot concentration at low pressure. In addition, the reduced pressure also seems to result in a more stable flame area as shown in Figure 5, again probably due to lower convection. Finally, as the droplet diameter decreases, less fuel vapor is generated by evaporation and the soot flame area tends to gradually decrease.

3.2.2. Effect of Puffing on Soot Characteristics. Due to the multi-component nature of RP-3, the phenomenon of puffing and generation of sub-droplets is present in the droplet combustion process. The high-speed camera captured the droplet puffing and sub-droplet generation as shown in Figure 6. A typical droplet puffing process consists of two main stages: bubble growth and puffing. First, the bubble grows in diameter after nucleation in the local superheated environment of the droplet. As the proportion of bubbles inside the droplet increases, the overall diameter of the droplet also grows, which is manifested by a jittering of the droplet D^2 curve, as mentioned in Figure 2a above. According to the d^2−law, the droplet evaporation mass rate is proportional to the diameter. The growth of droplet diameter brought by bubble growth increases the vapor mass flow rate. This leads to an increase in soot production, and higher carbon soot heights are observed at 1008.3−1054.3 ms in Figure 6a. The height grows until the droplet diameter reaches its maximum and blowout occurs. At 1054 ms, the droplet is ejected in the direction shown by the red arrow. The ignition of the ejected vapor disturbs the soot flame on the side of the jet. The soot formed by the sprayed vapor rises by natural convection and eventually detaches from the main body of the soot flame at the top. While the droplet diameter recovers after the vapor injection, the soot flame height also recovers to a height close to that before puffing.

Under the action of surface tension, puffing is often accompanied by the generation of sub-droplets. It is worth noting that some of the micron-sized sub-droplets produce carbon soot trails with high carbon soot concentration locally as shown in Figure 6b. However, this phenomenon rarely occurs; for example, the sub-droplets ejected upward into the main flame in Figure 6b do not produce similar soot trails. This is most likely due to the low oxygen content in the main flame that inhibits the high-intensity combustion of sub-droplets.

3.2.3. Soot Volume Fraction Distribution. Soot concentration distribution of the droplet flame under different pressures is shown in Figure 7. The height and area of the carbon soot flame can be found to increase and then decrease with the burning of the droplet, which is similar to that described in the previous section, and it was found that the decrease in pressure leads to a decrease in the height and an increase in the width of the soot flame. In the near atmospheric pressure environment, the soot flame distribution characteristics are close to the laminar diffusion flame, while the soot distribution changes significantly as the pressure decreases. The volume fraction of soot on the flame axis is shown below the picture in Figure 7. Zero point is defined as the position of the upper edge of the droplet. The concentration of soot in the droplet flame tends to increase and then decrease with increasing height. The height at which soot starts to be generated on the axis at each pressure is about 4 mm, while soot appears earlier at the beginning or end of the combustion period. At the same time, the pressure drop also significantly reduces the volume fraction of soot in the flame. In order to quantify this trend, the average value of the soot concentration on the flame was calculated and the results are displayed in Figure 8a. After the droplet ignition, the soot concentration shows a trend of increasing and then decreasing, corresponding to the (2) stable expansion and (3) reduction stages, respectively. However, unlike the flame area variation in Figure 5, the soot concentration reaches a higher level at ignition at 0.6−1.0 bar, about 70% of the maximum value, which is significantly higher than the concentration at the end of droplet combustion. This is mainly due to the fact that at the beginning of droplet combustion, collisions due to natural

https://doi.org/10.1021/acsomega.3c00655
ACS Omega 2023, 8, 14053−14065

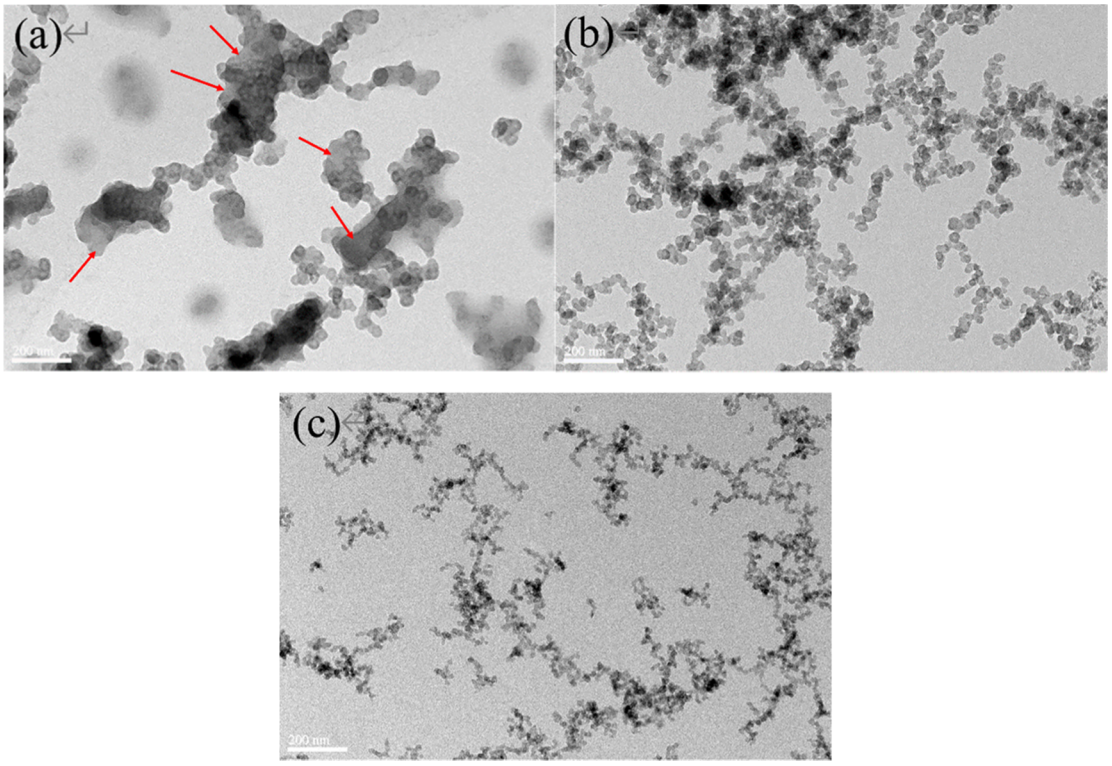

Figure 9. TEM images of soot agglomerates produced from RP-3 droplets at (a) 1.0 bar; (b) 0.6 bar; (c) 0.3 bar.

convection raise the soot concentration as shown in Figure 4. However, the natural convection is significantly suppressed below 0.4 bar. The overall change in soot concentration at 0.2−0.4 bar pressure is more stable, with soot concentration close to 0 after ignition. The soot concentration reaches a maximum in the middle of the droplet combustion history and then gradually decreases as the droplet diameter decreases, which is the same trend as the flame area.

The mean of soot concentration (f_v) in Figure 8b is obtained by averaging the data of Figure 8a with the standard deviation of the error bars. It can be found that the volume fraction of soot increases monotonically with increasing pressure. When the ambient pressure increases from 0.2 to 1.0 bar, the soot volume fraction increases by 2600% from 0.437 to 11.801 ppm. The relationship between f_v and P was fitted in the small window in Figure 8b, and a proportional relationship between f_v and $P^{2.044\pm0.066}$ was obtained.

3.2.4. Soot Morphology. Figure 9 shows TEM images of soot samples produced by RP-3 at 0.3−1.0 bar pressure. It can be seen that the soot aggregates are irregular in shape and consist of a number of spherical primary particles that form a "grape-like" structure. The size of soot particles is relatively large at 1.0 bar pressure, and the particles are very closely linked to each other. In addition to simple aggregation between particles, lamellar connections were also found, as shown by the red arrow in Figure 9a. At 0.6 and 0.3 bar pressure, the particle size of soot particles decreased significantly, the connection between particles was loose, and no lamellar connection structure between particles was found. This stronger lamellar linkage structure is likely to play a crucial role in the formation of the soot particle clusters shown in Figure 4. It helps form larger and tighter clusters of soot particles at 1.0 bar. The decrease in pressure results in the inhibition of this lamellar linkage and prevents the formation of particle clusters as observed in Section 3.2.1. Soot emissions depend on the competition between soot formation and soot oxidation.[25] The decrease in pressure also leads to a decrease in particle diameter, which helps to increase the specific surface area and oxidation activity of soot particles. Moreover, the drop in pressure leads to a slight increase in droplet flame temperature and more OH* generation observed in the previous study,[10] which are considered to be the main oxidizing agent of soot particles.[37,38] The above analysis shows that the sub-atmospheric environment inhibits the collision growth of soot particles, while the oxidation process of soot particles may be facilitated by a higher concentration of OH*, and under the combined influence of these factors, soot emissions show an exponential decrease. The size of the primary particles was determined by applying circular contours to the primary particles isolated on the TEM images, and the histogram distribution of the primary particle sizes under the various pressures is presented in Figure 10. For each pressure, approximately 200 particles were selected from different soot aggregates and different parts of the TEM grid to obtain the average diameter of the primary particles. As shown in Figure 11, the particle size distribution shifts toward a smaller size range as the pressure decreases, with average primary soot particles of 48.23, 35.426, 27.096, and 18.718 nm at 1.0, 0.6, 0.4, and 0.3 bar pressures, respectively. The very small size of soot particles produced by RP-3 single-droplet combustion at sub-atmospheric pressure is attributed to the fact that soot particle growth and collisions were suppressed at sub-atmospheric pressure. Combining the average carbon soot concentration and average particle size data, the number density of soot particles can be obtained by $N = f_v / \left(\frac{1}{6}\pi D_p^3\right)$. The results are shown in Figure 11, where the pressure variation has a small effect on the number density of soot

https://doi.org/10.1021/acsomega.3c00655
ACS Omega 2023, 8, 14053−14065

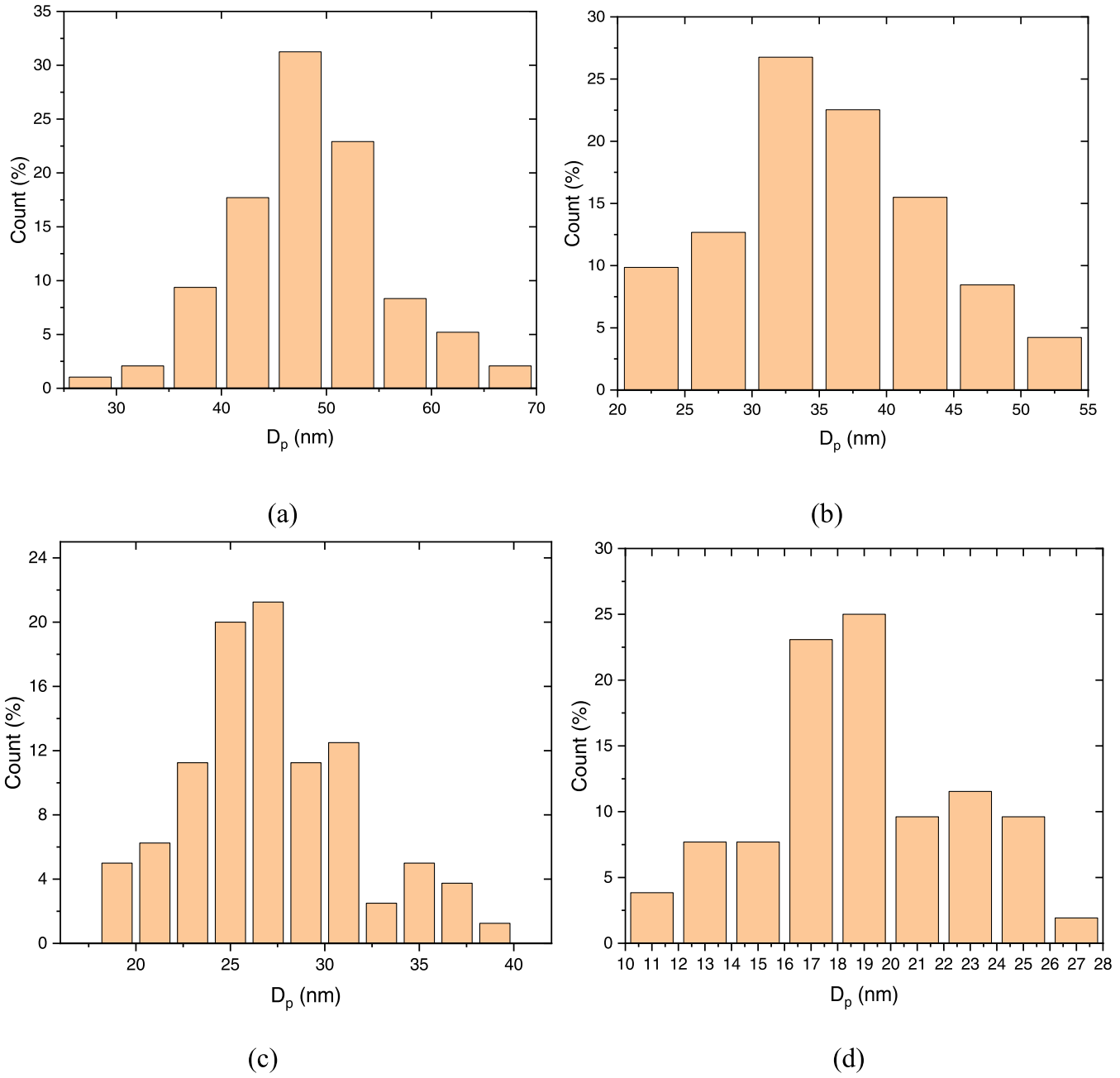

Figure 10. Histogram distributions of primary particle size of soot samples under (a) 1.0 bar; (b) 0.6 bar; (c) 0.4 bar; (d) 0.3 bar.

particles. It is revealed that the effect of sub-atmospheric environment on soot concentration is mainly achieved by reducing the particle diameter, while the effect on particle number density can be neglected.

4. CONCLUSIONS

The burning and soot characteristics of RP-3 kerosene were investigated under different sub-atmospheric pressures. The following conclusions can be drawn from this study:

The combustion rate decreases from 1.236 to 1.015 mm^2/s when the ambient pressure decreases from 1.0 to 0.4 bar, and the flame temperature is slightly decreasing with increasing pressure. Sub-atmospheric pressure environment significantly inhibits the formation of soot particle clusters during the ignition of the droplet, which is likely to benefit from the inhibition of particle lamellar junctions in a sub-atmospheric environment. The average soot volume fraction in the flame increases approximately with increasing pressure at 0.2−1.0 bar with a power of 2.044 ± 0.066. As the pressure decreases from 1.0 to 0.2 bar, the average soot volume fraction decreases significantly from 11.801 to 0.437 ppm. The analysis shows that this is mainly due to the fact that the sub-atmospheric environment not only inhibits the collisional growth of soot particles but also promotes the oxidation process of soot particles. The collected soot particles reveal a significant reduction in particle size under sub-atmospheric pressure with average primary soot particles of 48.23, 35.43, 27.096, and 18.718 nm at 1.0, 0.6, 0.4, and 0.3 bar pressures, respectively. It is revealed that the effect of sub-atmospheric environment on soot concentration is mainly achieved by reducing the particle diameter, while the effect on particle number density can be neglected.

https://doi.org/10.1021/acsomega.3c00655
ACS Omega 2023, 8, 14053−14065

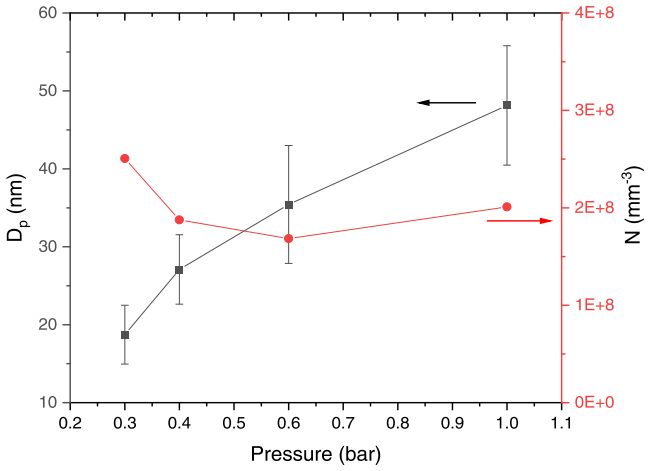

Figure 11. Average particle diameter (D_p) and number density (N) of soot particles at 0.3−1.0 bar.

AUTHOR INFORMATION

Corresponding Author

Zhihua Wang − *State Key Laboratory of Clean Energy Utilization, Zhejiang University, Hangzhou 310027, China; Key Laboratory of Clean Energy and Carbon Neutrality of Zhejiang Province, Hangzhou 310027, China;* orcid.org/0000-0002-7521-2900; Email: wangzh@zju.edu.cn

Authors

Jie Huang − *State Key Laboratory of Clean Energy Utilization, Zhejiang University, Hangzhou 310027, China*

Yong He − *State Key Laboratory of Clean Energy Utilization, Zhejiang University, Hangzhou 310027, China; Key Laboratory of Clean Energy and Carbon Neutrality of Zhejiang Province, Hangzhou 310027, China;* orcid.org/0000-0002-7037-9007

Hongtao Zhang − *Shanghai Institute of Space Propulsion, Shanghai 201112, China*

Yan Dai − *State Key Laboratory of Clean Energy Utilization, Zhejiang University, Hangzhou 310027, China*

Complete contact information is available at: https://pubs.acs.org/10.1021/acsomega.3c00655

Notes

The authors declare no competing financial interest.

ACKNOWLEDGMENTS

This work was supported by Zhejiang Provincial Natural Science Foundation (LZ21E06003), the National Natural Science Foundation of China (52125605), and the Fundamental Research Funds for the Central Universities (2022ZFJH004).

REFERENCES

(1) Krishnan, S.; George, P. Solid fuel ramjet combustor design. *Prog. Aeronaut. Sci.* **1998**, *34*, 219−256.

(2) Luo, W.; Pan, Y.; Tan, J.; Wang, Z. Experimental investigation on combustion efficiency of the ramjet model at low pressure. *J. Propul. Technol.* **2010**, *31*, 270−275.

(3) Ghassemi, H.; Baek, S. W.; Khan, Q. S. Experimental Study on Evaporation of Kerosene Droplets at Elevated Pressures and Temperatures. *Combust. Sci. Technol.* **2006**, *178*, 1669−1684.

(4) Khan, Q. S.; Baek, S. W.; Ghassemi, H. On the Autoignition and Combustion Characteristics of Kerosene Droplets at Elevated Pressure and Temperature. *Combust. Sci. Technol.* **2007**, *179*, 2437−2451.

(5) Kim, D. M.; Baek, S. W.; Yoon, J. Ignition characteristics of kerosene droplets with the addition of aluminum nanoparticles at elevated temperature and pressure. *Combust. Flame* **2016**, *173*, 106−113.

(6) Ghassemi, H.; Baek, S. W.; Khan, Q. S. Experimental Study on Binary Droplet Evaporation at Elevated Pressures and Temperatures. *Combust. Sci. Technol.* **2006**, *178*, 1031−1053.

(7) Hashimoto, N.; Nomura, H.; Suzuki, M.; Matsumoto, T.; Nishida, H.; Ozawa, Y. Evaporation characteristics of a palm methyl ester droplet at high ambient temperatures. *Fuel* **2015**, *143*, 202−210.

(8) Javed, I.; Baek, S. W.; Waheed, K. Evaporation characteristics of heptane droplets with the addition of aluminum nanoparticles at elevated temperatures. *Combust. Flame* **2013**, *160*, 170−183.

(9) Javed, I.; Baek, S. W.; Waheed, K. Autoignition and combustion characteristics of kerosene droplets with dilute concentrations of aluminum nanoparticles at elevated temperatures. *Combust. Flame* **2015**, *162*, 774−787.

(10) Zhang, H.; Wang, Z.; He, Y.; Xia, J.; Zhang, J.; Zhao, H.; Cen, K. Ignition, puffing and sooting characteristics of kerosene droplet combustion under sub-atmospheric pressure. *Fuel* **2021**, *285*, No. 119182.

(11) Huang, J.; Zhang, H.; He, Y.; Zhu, Y.; Wang, Z. Evaporation, Autoignition and Micro-Explosion Characteristics of RP-3 Kerosene Droplets under Sub-Atmospheric Pressure and Elevated Temperature. *Energies* **2022**, *15*, No. 7172.

(12) Suh, H. K.; Lee, C. S. A review on atomization and exhaust emissions of a biodiesel-fueled compression ignition engine. *Renewable Sustainable Energy Rev.* **2016**, *58*, 1601−1620.

(13) Johnson, T.; Joshi, A. In *Review of Vehicle Engine Efficiency and Emissions*, SAE Technical Paper Series; SAE Mobilus, 2017. DOI: 10.4271/2017-01-0907.

(14) Choi, J.; Yi, T.; Kim, H. Combustion of a dilute carbon black/ethanol nanofuel droplet in elevated pressure conditions. *Fuel* **2021**, *292*, No. 120376.

(15) Rasid, A. F. A.; Zhang, Y. Combustion characteristics and liquid-phase visualisation of single isolated diesel droplet with surface contaminated by soot particles. *Proc. Combust. Inst.* **2019**, *37*, 3401−3408.

(16) Jackson, G. S.; Avedisian, C. T.; Yang, J. C. Observations of soot during droplet combustion at low gravity: heptane and heptane/monochloroalkane mixtures. *Int. J. Heat Mass Transfer* **1992**, *35*, 2017−2033.

(17) Zhu, M.; Setyawan, H. Y.; Zhang, Z.; Zhang, D. Effect of n-butanol addition on the burning rate and soot characteristics during combustion of single droplets of diesel−biodiesel blends. *Fuel* **2020**, *265*, No. 117020.

(18) Zhu, M.; Ma, Y.; Zhang, Z.; Chan, Y. L.; Zhang, D. Effect of oxygenates addition on the flame characteristics and soot formation during combustion of single droplets of a petroleum diesel in air. *Fuel* **2015**, *150*, 88−95.

(19) Ojha, P. K.; Prabhudeva, P.; Karmakar, S.; Maurya, D.; Sivaramakrishna, G. Combustion characteristics of JP-10 droplet loaded with Sub-micron boron particles. *Exp. Therm. Fluid Sci.* **2019**, *109*, No. 109900.

(20) Shang, W.; Yang, S.; Xuan, T.; He, Z.; Cao, J. Experimental Studies on Combustion and Microexplosion Characteristics of N-Alkane Droplets. *Energy Fuels* **2020**, *34*, 16613−16623.

(21) Dasch, C. J. One-dimensional tomography: a comparison of Abel, onion-peeling, and filtered backprojection methods. *Appl. Opt.* **1992**, *31*, 1146−1152.

(22) He, Y.; Qi, S.; Liu, S.; Xin, S.; Zhu, Y.; Wang, Z. Effects of the Gas Preheat Temperature and Nitrogen Dilution on Soot Formation in Co-flow Methane, Ethane, and Propane Diffusion Flames. *Energy Fuels* **2021**, *35*, 7169−7178.

(23) Qi, S.; Sun, Z.; Wang, Z.; Liu, Y.; He, Y.; Liu, S.; Wan, K.; Nathan, G. J.; Costa, M. Effects of gas preheat temperature on soot

https://doi.org/10.1021/acsomega.3c00655
ACS Omega 2023, 8, 14053−14065

formation in co-flow methane and ethylene diffusion flames. *Proc. Combust. Inst.* **2021**, *38*, 1225−1232.
(24) Schulz, C.; Kock, B. F.; Hofmann, M.; Michelsen, H.; Will, S.; Bougie, B.; Suntz, R.; Smallwood, G. Laser-induced incandescence: recent trends and current questions. *Appl. Phys. B* **2006**, *83*, 333−354.
(25) Karataş, A. E.; Gülder, Ö. L. Soot formation in high pressure laminar diffusion flames. *Prog. Energy Combust. Sci.* **2012**, *38*, 818−845.
(26) Joo, H. I.; Gülder, Ö. L. Soot formation and temperature field structure in co-flow laminar methane−air diffusion flames at pressures from 10 to 60atm. *Proc. Combust. Inst.* **2009**, *32*, 769−775.
(27) Liu, F.; Daun, K. J.; Beyer, V.; Smallwood, G. J.; Greenhalgh, D. A. Some theoretical considerations in modeling laser-induced incandescence at low-pressures. *Appl. Phys. B* **2007**, *87*, 179−191.
(28) Zhang, C.; Wu, Y.; Liu, B.; Wang, Z.; Zhou, L. Investigation of soot particles morphology and size distribution produced in a n-heptane/anisole laminar diffusion flame based on TEM images. *Combust. Flame* **2022**, *244*, No. 112234.
(29) Vargas, A. M.; Gülder, Ö. L. Pressure dependence of primary soot particle size determined using thermophoretic sampling in laminar methane-air diffusion flames. *Proc. Combust. Inst.* **2017**, *36*, 975−984.
(30) Yang, B.; Hu, B.; Koylu, U. O. Mean soot volume fractions in turbulent hydrocarbon flames: A comparison of sampling and laser measurements. *Combust. Sci. Technol.* **2005**, *177*, 1603−1626.
(31) Chandler, M. F.; Yingwu, T.; Koylu, U. O. Diesel engine particulate emissions: A comparison of mobility and microscopy size measurements. *Proc. Combust. Inst.* **2007**, *31*, 2971−2979.
(32) Flower, W. L.; Bowman, C. T. Measurements of the structure of sooting laminar diffusion flames at elevated pressures. *Symp. Int. Combust.* **1985**, *20*, 1035−1044.
(33) Zhang, Y.; Huang, R.; Wang, Z.; Xu, S.; Huang, S.; Ma, Y. Experimental study on puffing characteristics of biodiesel-butanol droplet. *Fuel* **2017**, *191*, 454−462.
(34) Ma, Y.; Zhu, M.; Zhang, Z.; Zhang, D. Effect of a homogeneous combustion catalyst on the nanostructure and oxidative properties of soot from biodiesel combustion in a compression ignition engine. *Proc. Combust. Inst.* **2015**, *35*, 1947−1954.
(35) Leschowski, M.; Dreier, T.; Schulz, C. An automated thermophoretic soot sampling device for laboratory-scale high-pressure flames. *Rev. Sci. Instrum.* **2014**, *85*, No. 045103.
(36) LAW, C. K. Recent advances in droplet vaporization and combustion. *Prog. Energy Combust. Sci.* **1982**, *8*, 171−201.
(37) Fenimore, C. P.; Jones, G. W. Oxidation of soot by hydroxyl radicals. *J. Phys. Chem. A* **1967**, *71*, 593−597.
(38) Haynes, B. S.; Wagner, H. G. Soot formation. *Prog. Energy Combust. Sci.* **1981**, *7*, 229−273.

https://doi.org/10.1021/acsomega.3c00655
ACS Omega 2023, 8, 14053−14065